Chapter 4B

Projection Systems for Extreme Ultraviolet Lithography

Russell M. Hudyma and Regina Soufli

Contents

4B.1 General EUVL Optical Design Considerations

All projection optics in an EUV lithography (EUVL) system must be reflective and are coated with thin films consisting of alternating layers of materials termed "multilayers (MLs)," at a total thickness of about 280 nm. These coatings act as Bragg reflectors and are designed to operate at the EUVL wavelengths of illumination (centered at ∼13.4 to 13.5 nm) at near-normal-incidence angles. The ability to deposit such highly reflective ML coatings with extremely precise thickness control across the optic surface (in order to preserve the optic figure) has been the enabling technology for EUVL. Since ML coatings are essential, every EUVL projection system must be ML-compatible. The theoretical reflectance properties of a normal-incidence molybdenum-silicon (Mo/Si) ML suited for EUVL are shown in Fig. 4B.1.

In a poorly designed EUV projection system, MLs can induce appreciable amplitude and phase errors at the exit pupil of the image system. In an uncompensated design, the ML-induced phase error can easily exceed 4 to 5 times the residual

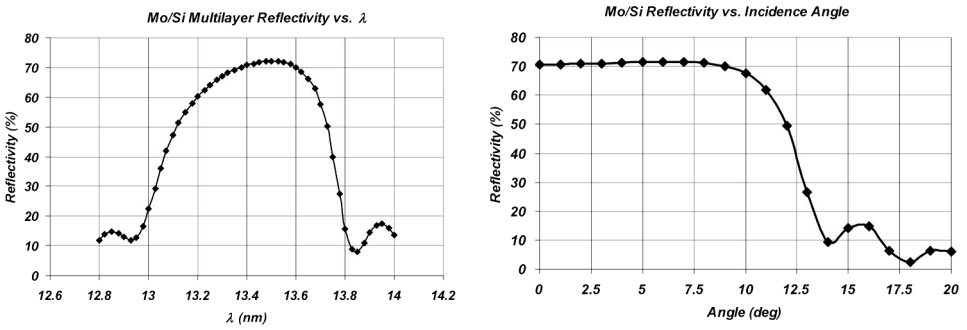

Figure 4B.1 Normal-incidence reflectivity vs wavelength and reflectivity vs angle for an ideal Mo/Si ML with 40 bilayer pairs. The period of a single bilayer is 7.0 nm and the thickness of individual Mo and Si layers is 2.76 nm and 4.14 nm, respectively.

wavefront error of the uncoated system. Amplitude effects are equally important; a poorly designed system will have appreciable apodization across the exit pupil, leading to poor critical dimension (CD) uniformity across the field and telecentricity errors at the wafer for any single field point. There are no rigorous rules to ensure ML compatibility. But a guiding principle is that stringent controls on both the mean incidence angle on each mirror, as well as the range of incidence angles as seen from any point on the mirror, must be enforced.[1–5]

As with other lithographic technologies, EUVL strives to achieve continuous improvements in resolution, thus enabling smaller device geometries.[5] This is accomplished fundamentally by increasing the numerical aperture (NA) of the projection optics, which creates an interesting coupled set of technology problems to solve: (1) the synthesis of EUVL projection optics forms with large NAs (NA $>$ 0.25) and beyond, and (2) the development of a ML coating design set capable of supporting basic imaging at this increased NA. Recent work has demonstrated that EUVL designs with NAs in excess of 0.40 can be synthesized using relatively deep aspheric mirrors with large aspheric gradients. It has also been demonstrated that these systems will support ML imaging at 4$\times$ or even 5$\times$ reduction.[7]

The synthesis of these high-NA systems follows five basic steps:

1. The synthesis of all-reflective or catoptric projection system concepts capable of correcting imaging aberrations at NAs in excess of 0.25 over meaningful slit widths with an even number of reflections.
2. The characterization and correction of ML-induced amplitude errors at high NA.
3. The characterization and correction of ML-induced phase errors at high NA.
4. The simultaneous refinement of the complete projection systems (optics and ML coatings) via damped least squared (DLS) optimization using specialized user-defined error functions.

5. A validation, via an analysis of the partial coherent imagery, that the canonical projection systems can meet lithographic imaging standards.

This process flow is illustrated in Fig. 4B.2.

Since EUVL projection systems are all-reflective, there are several additional subtleties beyond simple ML compatibility and the dual-track optimization process to achieve a manufacturable solution. The aspheric mirrors used in an EUVL projection system must have both the peak departures and aspheric gradients carefully controlled to ensure *both* the fabrication and metrology process. First, the absolute aspheric departure from the best-fit sphere sets the maximum number of fringes that the interferometer must accommodate. As the maximum number of fringes increases, the complexity of the compensation optics used to "null" the test wavefront generally increases. Second, the peak aspheric departure is a measure of the material that must be removed during the fabrication process. Since this removal process is performed with sub-aperture tools, excessive departures lead to excessive process times, which add to the risk of introducing mid-spatial-frequency errors due to process fluctuations.

Perhaps even more important than the maximum aspheric departure is the aspheric gradient, or the change in aspheric sag as a function of lateral coordinates across the mirror surface. This sets the local fringe density that the

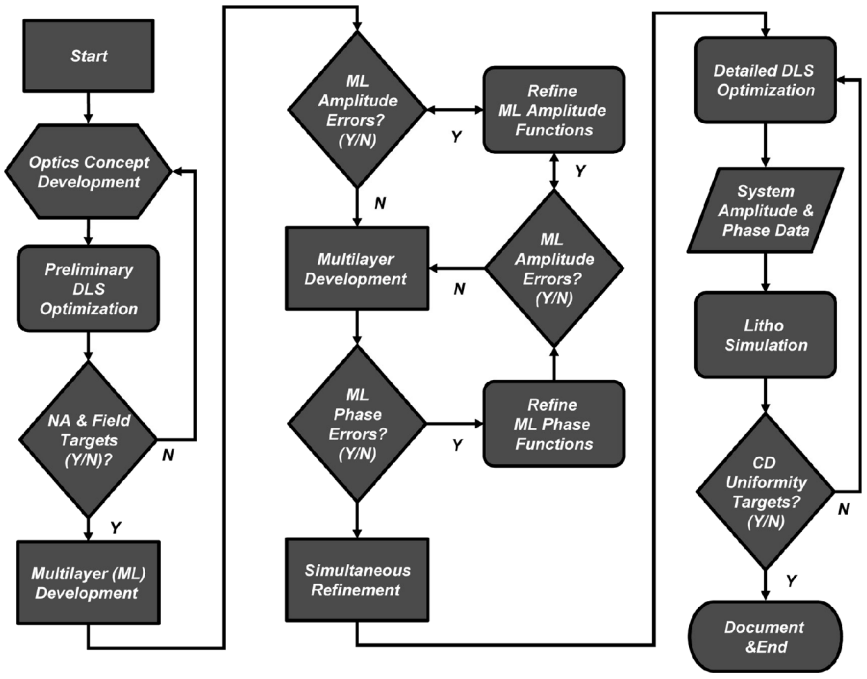

Figure 4B.2 Necessary process flow to determine the extensibility of EUVL. The process starts by conceptualizing canonical EUV projection systems targeted at process nodes down to 15 nm. The remaining tasks determine if these conceptual systems are (1) compatible with EUV MLs and (2) support lithographic-quality imaging.

interferometer's sensor must resolve. At an empirical limit of approximately four pixels per fringe, the interferometry simply no longer has the accuracy with which to test the EUV surfaces. And to generate steeper gradients, higher-frequency tool functions in the polishing process are required. These higher-frequency tool functions have the tendency to increase the mid-spatial-frequency roughness (MSFR). To compound the problem, mid-spatial-frequency smoothing techniques do not work as well in regions of increased mirror slope.

In addition to ML compatibility and the challenges of essentially tailoring aspheric mirrors that need to be figured to atomic dimensions, EUVL systems have the usual challenges related to the development of multimirror systems, including ray clearance, back working distance, volume claims for mounting interface, etc. Working distances and clearances are also driving issues, since mirror substrates need adequate thickness to overcome mount-induced deformations.

Despite these challenges, EUV projection systems are a reality today, and several high-profile systems are enabling EUV researchers to continue to unlock the promise of EUV technology.

4B.2 EUV Microsteppers

The semiconductor industry uses a reduced field image size at a similar optical resolution to that eventually intended to be adopted in production, and microsteppers to gain early learning on new technology nodes four to five years ahead of their introduction. Microsteppers allow manufacturers and researchers alike to develop and qualify new photoresists well before they are required for high-volume integrated circuit (IC) manufacturing. Microsteppers also allow researchers to investigate defect printability, test new reticle designs, and fabricate prototype ICs at the node of interest as well as provide early learning on tool-related technology challenges associated with sources, optics, lens aberrations, imaging effects, materials, metrology, reticles, photoresists, contamination, cost of ownership, reliability, and lifetime. In the field of EUV, both the "10×" microstepper and microexposure tool (MET) have played pivotal roles in the development of EUV technology and infrastructure.

4B.2.1 "10×" microstepper

Between 1997 and 2002, EUVL was given a tremendous technology push with developments made by the Virtual National Laboratory (VNL), which consists of Lawrence Livermore, Sandia, and Lawrence Berkeley National Laboratories (LLNL, SNL, and LBNL, respectively). Funding was supplied by the EUV Limited Liability Company (LLC)—a consortium formed by IC manufacturers Intel, AMD, IBM, Infineon, Micron, and Motorola. Much of the initial technology development work was performed using what was called the "10×" microstepper.[8]

The 10× projection optics consist of a two-mirror objective arranged in a Schwarszchild form with a convex primary mirror and a concave secondary mirror, as light travels left to right from the patterned mask to the wafer. This objective is of the reverse telephoto type so that the back working distance is greater than the focal length of the objective. The projection optics were designed with a maximum centered NA of 0.30, but the aperture stop is decentered to produce a system with an unobscured circular aperture (Fig. 4B.3). The geometry constraints imposed by reasonable opto-mechanical considerations limit the NA of the off-axis bundle to 0.088 by design.

For an object at infinity, the Schwarzschild objective is formed by two concentric spherical mirrors. The design is free from spherical aberration, coma, and astigmatism, provided that the ratio of concave radius to the convex radius (R_2/R_1) is equal to $(\sqrt{5}+1)/(\sqrt{5}-1)$ or 2.618034. When the system is used in a microstepper at a reduction ratio, the object distance must be given some finite value. This means that the concave secondary mirror must be weakened to correct the spherical aberration and coma while maintaining the concentricity of the mirrors M1 and M2. For this 10× objective, the new R_2/R_1 ratio is 3.083498, which is in close agreement to an example provided by Kingslake.[9] The resulting objective is free from spherical aberration, coma, and astigmatism at 0.088 NA, with the field curvature limiting the imaging performance. The residual root mean square (rms) composite wavefront error within a 280-μm square field of view as-designed is 0.055λ (λ = 13.4 nm), or 0.75 nm. The inward field curvature is approximately 0.80 μm when analyzed across the 400-μm-diameter field. These parameters are summarized in Table 4B.1.

The 10× microstepper received an upgraded optics package in late 1998, with the figure error of both primary and secondary mirrors approaching 0.4-nm rms. By clocking the mirrors relative to each other, the subaperture wavefront was optimized to achieve a residual rms wavefront error of 0.045λ (0.6 nm). This rms value was derived from a 37-term Zernike expansion to the measured interferogram, representing an as-built wavefront error value that was actually *lower* than the design residual. In addition to the excellent mirror figure, the MSFR (mid-spatial frequency roughness corresponding to spatial periods of 1 mm^{-1} to 1 μm^{-1}) achieved

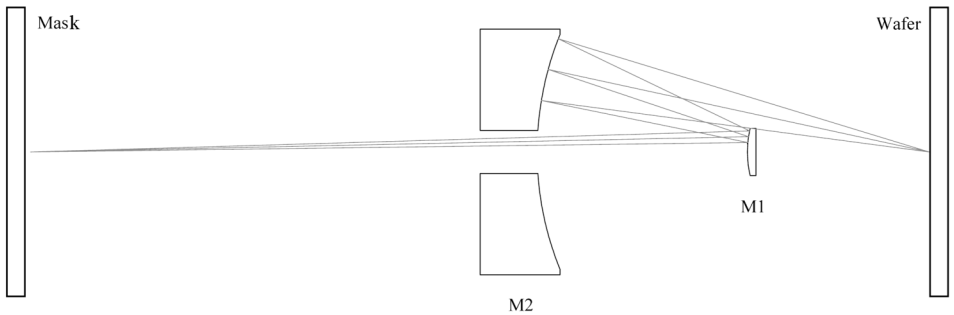

Figure 4B.3 10× microstepper projection optics illustrating the decentered aperture stop on the primary mirror M1.

Table 4B.1 10× microstepper design parameters.

Parameter	Value
Wavelength	13.4 nm
Numerical aperture (NA)	0.088 (circular stop) 0.088 × 0.10 (rectangular stop)
Reduction ratio	10×
Field format	283 × 283 μm square (400-μm diagonal)
Residual rms wavefront error	0.055λ
Total track	315.2 mm
Demonstrated resolution	70 nm 1:1 L/S

on both the primary and secondary mirrors was 0.13-nm rms and 0.20-nm rms, respectively. These MSFR values enabled low-flare imaging with measured flare levels on the order of 4%. Subsequent printing experiments in 1999 at the VNL demonstrated high-fidelity iso-dense elbows at both 90 nm and 80 nm using the circular 0.088-NA aperture set. Using the 0.10 × 0.088 NA rectangular aperture, a 70-nm L/S (lines and spaces) at a 1:2 pitch and a 1:1 pitch were patterned in a customized thin layer (80 to 100 nm) deep ultraviolet (DUV) resist.[8] These results were significant at the time because they established a k_1 factor of 0.52 for this process, which foreshadowed the potential for sub-30-nm resolution for a projection system designed with a NA of 0.30, which is going to be discussed in Sec. 4.B.2.2.

Yet another upgraded set of 10× microstepper optics was manufactured in 2002 to support a set of frequency-doubling experiments at LBNL's Advanced Light Source (ALS). The spatial frequency-doubling technique utilized a 40 μm × 40 μm silicon nitride (Si_3N_4) transmission grating with an aperture stop that was designed to block or "filter" the zero diffraction order from this grating. Essentially, the technique works by allowing the +1 and −1 diffraction orders to propagate through the optical system, interfering at the image plane. In this manner, a high-contrast spatial frequency doubled image of the grating pitch is produced. The researchers at LBNL were able to print high-quality 50-nm line/space patterns in Shipley's "EUV-2D" resist and quantify the line edge roughness (LER) of these printed images.[10]

4B.2.2 Microexposure tool (MET)

It became clear at the VNL that an upgraded micro-exposure capability was needed to demonstrate the full potential of EUVL to a 30-nm half-pitch. Based on some simple work with the lithographic scaling laws, it was decided that this new MET would have a NA of about 0.3, similar to the NA for a commercial alpha-tool, but substantially larger than both the 0.10 NA for the Engineering Test Stand (ETS) and 0.088 NA for the existing 10× microstepper.

The idea of employing a two-mirror aspheric imaging system has been proposed in earlier reports.[11,12] To achieve the largest possible field of view, the MET

projection optics utilize a primary and a secondary mirror whose radii are nearly the same (within 10% of each other). This enables the field curvature to be corrected to a value approaching that of more sophisticated multi-mirror EUVL projection systems. Compared to the 10× imaging system that uses the same field size at the wafer, this "equal radii" concept reduces the longitudinal field curvature from 1.8 μm to 0.05 μm. This 36-fold reduction in field curvature enables a 50% increase in printed field area per exposure relative to the 10× microstepper (Fig. 4B.4). The MET projection optics are designed to accommodate either a transmission mask (TM) or reflection mask (RM), with a depth of focus that can accommodate subtle tilts of the wafer up to ∼1 deg. With a RM, imaging is controlled by the Scheimpflug condition, which states that the imaging properties of a centered optical system with a tilted object are preserved on a tilted image plane (ignoring distortion). For a system used at finite conjugates, the image plane tilt is the object plane tilt scaled by the reduction ratio. A reflective mask can be tilted up to ∼5 deg in the MET.

Layouts of the final optical design with reflection and transmission masks are shown in Figs. 4B.5 and 4B.6, respectively. Table 4B.2 summarizes the performance of the optical design relative to parameter goals. A large NA of 0.30 is attained by the use of a centered design, where the imaging bundles are centered on the optical axis. The centered design necessitates that the image passes through a hole in the primary mirror. Eccentric or off-axis pupil design forms are not feasible

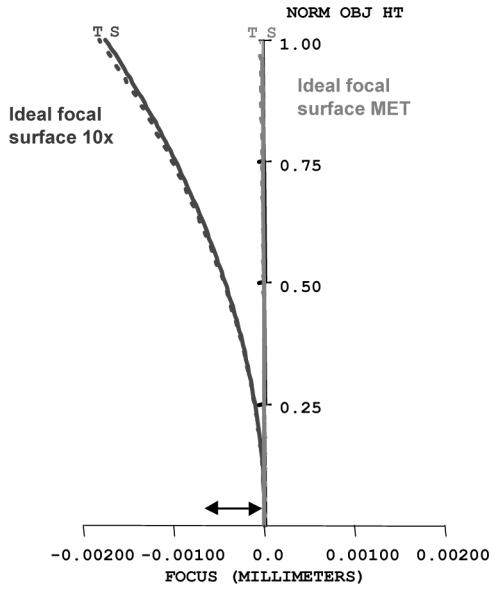

Figure 4B.4 The principal feature of the MET design is the reduction in field curvature, which allows focus to be maintained across the entire tilted wafer plane. The image formed at the wafer with the 10× camera would be outside the depth of focus due to the curvature of field. The *y*-axis is normalized to the field height of the MET (3 mm), which represents the field of view at the reticle that is projected at 5× reduction at the wafer. Both tangential (T, dashed line) and saggital (S, solid line) field curvatures are shown.

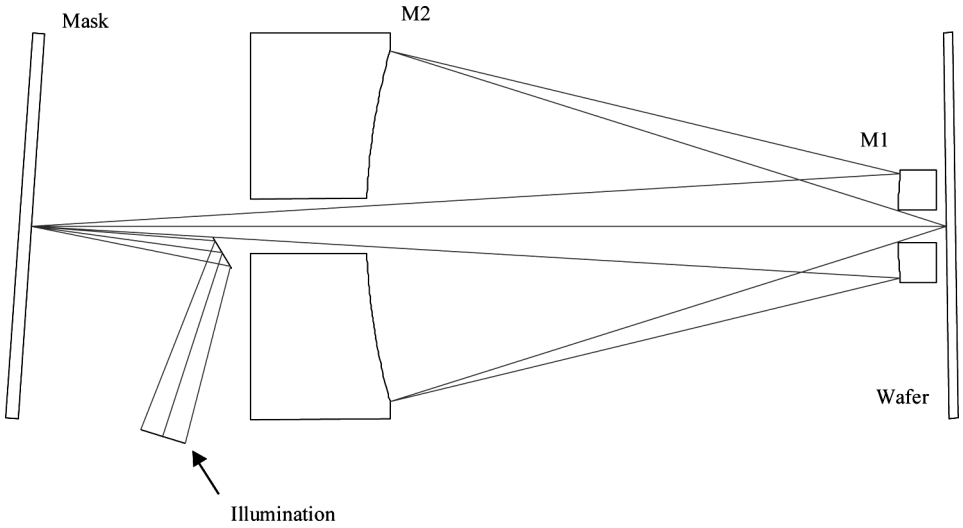

Figure 4B.5 Tilting the mask and wafer planes enables use of a reflection mask. In this embodiment, the mask is tipped by 4.0 deg, with a corresponding wafer tilt of 0.8 deg. The imagery is diffraction-limited on the tilted wafer plane.

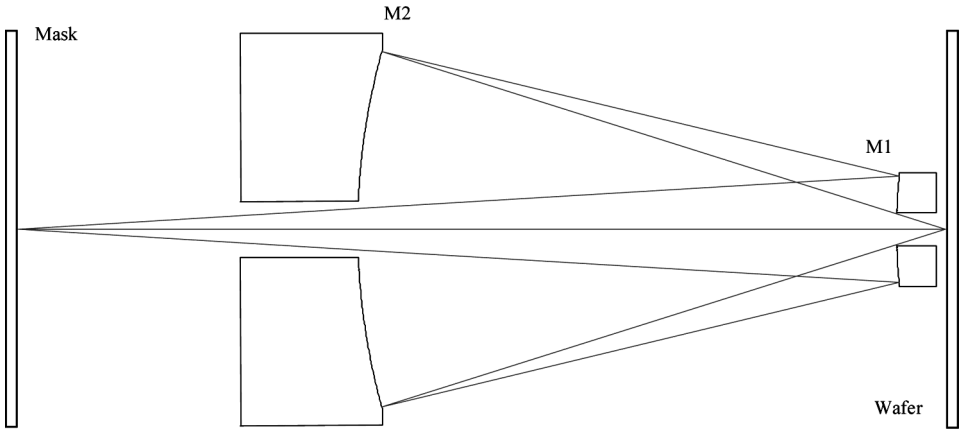

Figure 4B.6 "Equal radii" microstepper concept for use with a transmission mask. The design has a NA of 0.30 at a reduction of 5× as measured at the plane of the wafer. Mirror radii R1 and R2 are nearly the same, acting to minimize field curvature across the projected format.

because the individual mirrors work at very fast conjugates. The residual aberrations simply grow too quickly to correct as the pupil moves off the optical axis. This fact forces the central obscuration on the exit pupil of the imaging system. To minimize the obscured pupil area ($<10\%$), the image plane must be kept close to the primary mirror. This reduces the clearance between the back of the primary mirror and the wafer. The vertex thickness of the primary mirror was set to 20 mm to provide ample substrate stiffness, leaving only 5 mm of clearance between the

Table 4B.2 MET projection optics performance summary (RM = reflection mask, TM = transmission mask).

Parameter	Predicted performance
Wavelength	13.4 nm
Numerical aperture	0.30
Focal length	102.5 mm
Field format	
Type	Rectangular
Length × width	600 μm × 200 μm
Mask compatibility	RM & TM
Reduction ratio (nominal)	5:1
Residual rms wavefront error (waves @ $\lambda = 13.4$ nm)	
Field point maximum	0.054λ RM)
	0.027λ (TM)
Composite	0.031λ (RM)
	0.021λ (TM)
Resolution	30 nm
Distortion (peak-to-valley static, nm)	
Chief ray	497.6 nm (RM)
	2.24 nm (TM)
Depth of focus	200 nm
Telecentricity error	
Δy (nm) image/Δz (nm) focus	0.0148 nm/nm
Package	
Total track (mask/wafer)	474.16 mm
Overall length (vertex/vertex)	275.60 mm
Working distances	
M1/wafer	∼5.0 mm
M2/mask	∼113.56 mm
Aperture stop	Accessible on M1
Peak aspheric departure	
M1 (primary)	3.82 μm
M2 (secondary)	5.61 μm
Maximum aspheric slope	
M1 (primary)	−1.18 μm/mm
M2 (secondary)	−0.47 μm/mm
Angles of incidence, from normal	
M1 (max/min)	8.67°/2.54°
M2 (max/min)	1.98°/0.67°

back of the primary mirror and the wafer. This makes mechanical packaging of the primary mirror difficult and precludes the use of a grazing-incidence focus system.

While the limited clearance makes the mechanical design more complicated, this issue is manageable. The working distance is, in fact, about the same as for contemporary DUV steppers. The final design shown in Fig. 4B.5 includes a proposed mirror substrate thickness to help visualize clearance at the wafer and depict how the illumination is brought onto the mask. The design is optimized to work at a 5× reduction across a rectangular field of view of 600 × 200 μm^2 at the wafer. While the field could be extended in the long dimension, the aspect ratio of 3:1 will

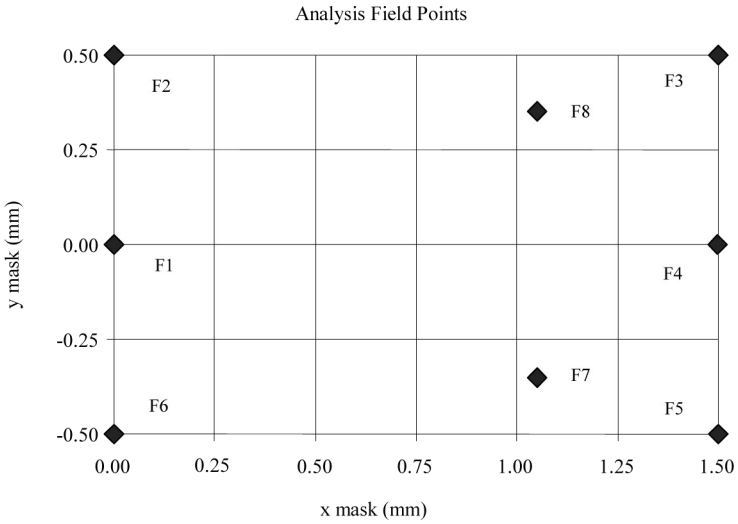

Figure 4B.7 Analysis field points for the computation of rms wavefront error, incoherent square wave modulation transfer function (MTF), and 2D/3D partially coherent imagery, for the MET tool. With a reflection mask, the printed field has bilateral symmetry, so only field points across the half-format need to be analyzed.

help to simplify the design of the illumination system. The mask is tilted clockwise at 4.0 deg; the wafer has a corresponding counterclockwise tilt of 0.8 deg. This is the minimum tilt required to avoid interference between the incoming illumination and imaging bundle.

With a RM, the composite rms wavefront error across a 600×200 μm^2 rectangular field is 0.42 nm (0.031λ). This compares favorably to the composite rms wavefront of 0.28 nm (0.021λ) with a TM. The difference between the two imaging conditions is that the wavefront error varies more across the tilted conjugate planes. With a RM, the wavefront error varies from 0.24 nm (0.018λ) to 0.74 nm (0.055λ). The wavefront error variation with a TM is 0.15 nm (0.011λ) to 0.36 nm (0.027λ). While this variation across a tilted wafer would be troublesome in a production tool, causing field-dependent CD variations across the field, it is not a significant issue for this R&D tool.

Since the MET projection optics are compatible with either a RM or a TM, the wavefront error and distortion analysis is performed in both modes of operation. The rms wavefront error was analyzed at nine distinct field points across the half-format as shown in Fig. 4B.7. This sampling is sufficient since the design has bilateral symmetry. The field size is set in RM mode because the maximum rms wavefront error at all field points must be less than 0.050λ. The rms wavefront error, less tilt, for each field point is listed in Table 4B.3. Using a TM, the field composite rms wavefront error is 0.28 nm (0.021λ). Residual field curvature and astigmatism present in the design cause a slight variation in the residual wavefront error across the field. With a RM, the field composite rms wavefront is 0.42 nm (0.031λ). There is more variation in the wavefront error in this case, due

Table 4B.3 Rms wavefront error (WFE) for the MET projection system, with tilt removed.

Field	x (mm)	y (mm)	rms WFE (TM)	rms WFE (RM)
F1	0.00	0.00	0.022λ	0.022λ
F2	0.00	0.50	0.018λ	0.046λ
F3	1.50	0.50	0.027λ	0.020λ
F4	1.50	0.00	0.022λ	0.024λ
F5	1.50	−0.50	0.027λ	0.054λ
F6	0.00	−0.50	0.018λ	0.018λ
F7	1.05	−0.35	0.011λ	0.024λ
F8	1.05	0.35	0.011λ	0.023λ
		Composite	0.021λ	0.031λ

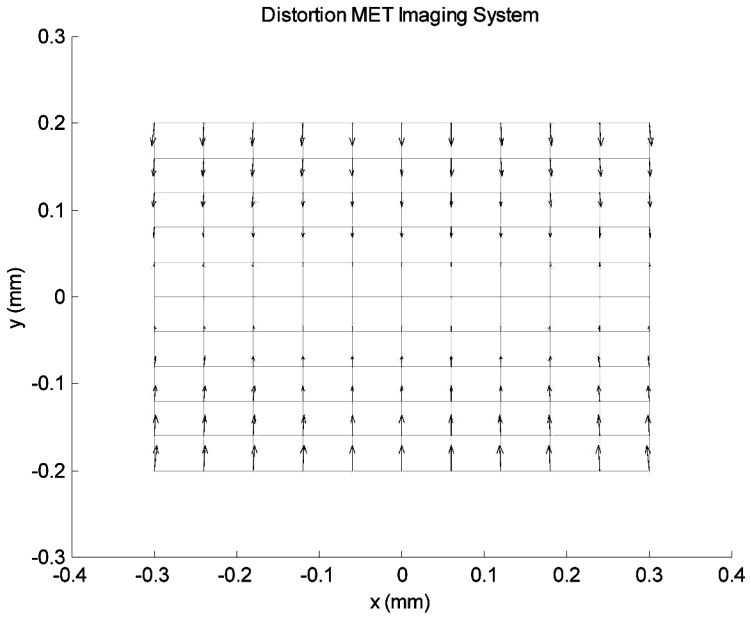

Figure 4B.8 Vector visualization of MET distortion using a TM over a 600 × 200 μm^2 imaging field at the wafer. The maximum radial distortion is only 2.24 nm. Since the system is rotationally symmetric in this mode of operation, the distortion field has rotational symmetry about the optical axis.

primarily to a variation in spherical aberration (fringe Zernike term Z9) across the field. This is a subtle effect that can be understood in the following way: with a tilted mask plane, the distance from the object surface to the first principal plane varies across the field, creating a field-dependent conjugate shift. Since the spherical aberration varies with conjugate distance, the spherical aberration will have field dependence.

Figures 4B.8 and 4B.9 graphically depict the distortion at the wafer with a TM and RM, respectively. The distortion vector field is superimposed on top of the ideal image grid. Even though this research tool requires an overlay, users must still understand the distortion fields in both imaging modes to address such issues

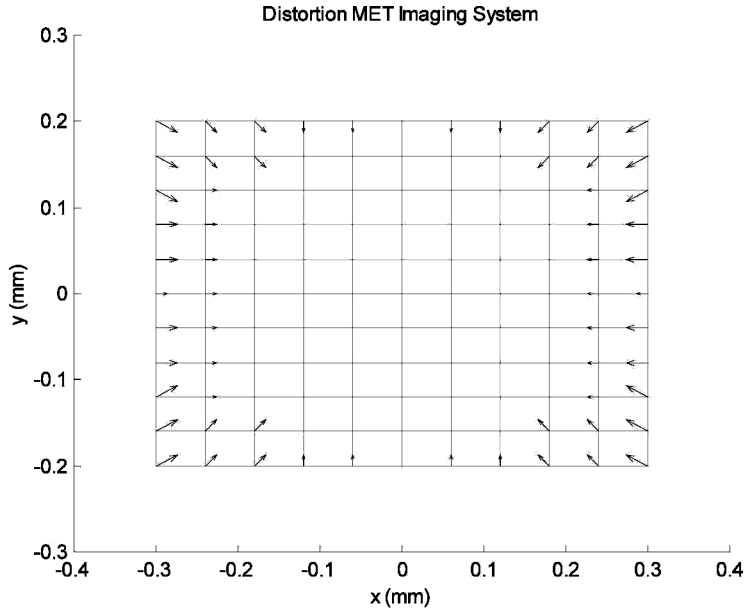

Figure 4B.9 Vector visualization of MET distortion using a RM over a 600×200 μm^2 imaging field at the wafer. In this case, the maximum radial distortion is $\sim$244 nm. The printed image suffers primarily from anamorphic distortion, which can be viewed simply as a foreshortening of the vertical dimension. Keystone distortion can also be seen in the vector field plot. Both forms of distortion are artifacts of imaging under the Scheimpflug condition.

as horizontal/vertical bias with tilted-plane imaging, and the potential to use this design in a scanning configuration.

With the TM situated perpendicular to the optical axis, the distortion field exhibits simple barrel distortion with rotational symmetry about this axis (Fig. 4B.8). The length of the largest distortion vector (and hence the maximum radial distortion) is 2.24 nm, with maxima being located in the corners of the format. There are no degrees of freedom in the optical design to correct distortion effectively; the distortion is minimized only because the projected field of view is small. An analysis of the scanned imagery shows an image placement error of $\sim$2 nm in the cross-scan dimension. The residual distortion is small enough to consider the possibility of using this design with a TM in a scanning configuration.

The behavior of the distortion field is much more complex with a RM (Fig. 4B.10). The printed image suffers primarily from anamorphic distortion ($\sim$200 nm), which can be viewed as a foreshortening of the vertical dimension due to the tilted plane. Keystone distortion ($\sim$30 nm) can also be seen in the vector field plot, which relates to the variation in magnification with conjugate distance from the mask to the first principal plane. Both forms of distortion are artifacts of imaging using tilted conjugate planes, and they combine to make a rectangular object imaged into an isosceles trapezoid. The longest distortion vector in the field plot is $\sim$240 nm in length. Barrel distortion is also present, but it is overwhelmed

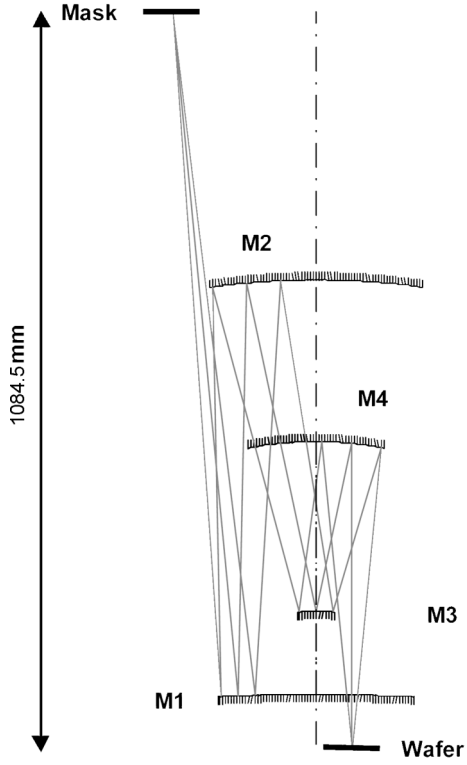

Figure 4B.10 Layout of the ETS projection optics (with full parents) that shows the imaging bundle from the mask (top) to the wafer (bottom). In practice, only off-axis sections of the mirrors are used, making the mirrors much smaller than shown in the figure. The aperture stop is fully accessible and located on mirror M3. Mirror M4 makes the imaging bundle perpendicular to the wafer plane, producing the telecentric design at this location.

by the other distortion forms. The conclusion of this analysis is that the MET camera is not suited for use in a scanning tool using a RM.

The optical design analysis and ML coating results from the first two MET cameras (set 1 and set 2) constructed at the VNL are described in Ref. 13. The set 2 MET camera is currently installed at the ALS synchrotron at LBNL and remains the most accurate micro-field, high-NA EUVL camera to date.[14–16]

4B.3 Engineering Test Stand (ETS)

The imaging performance specifications for the EUVL projection optics parallel those of other optical lithographies. The principal difference is that the specifications are scaled to reflect the 100-nm CD for the first-generation EUVL systems. The first prototype 0.1-NA, scanning EUVL system was constructed by the VNL. The top-level imaging specifications for the ETS system were:

1. 100-nm CD (70 nm for isolated features) based on NA $= 0.1$, $k_1 = 0.77$, and coherence factor $\sigma = 0.7$;